Multi-directional Ankle Impedance During Standing Postures

Guilherme A. Ribeiro, Lauren N. Knop, and Mo Rastgaar, Member, IEEE

Abstract— In this study, we estimated the multi-directional ankle mechanical impedance in two degrees-of-freedom (DOF) during standing, and determined how the stiffness, damping, and inertia vary with ankle angle and ankle torque at different postures. Fifteen subjects stood on a vibrating instrumented platform in four stationary postures, while subjected to pulse train perturbations in both the sagittal and frontal planes of motion. The four stationary postures were selected to resemble stages within the stance phase of the gait cycle: including post-heel-strike during the loading response, mid-stance, post-mid-stance, and just before the heel rises from the ground in terminal-stance phase. In general, the ankle stiffness and damping increased in all directions as the foot COP moved forward, and more torque is generated in plantarflexion. Interestingly, the multi-directional ankle impedance during standing showed a similar shape and major tilt axes to the results of non-loaded scenarios. However, there were notable differences in the impedance amplitude when the ankle was not under bodyweight loading. Last, the stiffness during standing had similar amplitudes ranges to the time-varying ankle stiffness during the stance phase of dynamic walking estimated in previous studies. These results have implications on the design of new, less physically intense, biomechanics experiments aimed at people with neuromuscular disorders or other physical impairments who cannot complete a standard gait test.

Index Terms— Biomechanics, human ankle, multi-directional ankle impedance, ankle neuromuscular characteristics, standing posture

I. INTRODUCTION

RECENT advancements in robotic technologies have led to the development of assistive and rehabilitation devices used to help human locomotion and improve performance during activities of daily living for both impaired and unimpaired people. The improvement of the design and control of these devices requires a comprehensive understanding of how the human ankle functions during different interactions with the environment. When the foot contacts the ground during walking, the ankle is subjected to the various ground reaction forces and torques and respond appropriately to these external disturbances [1]. A common method to characterize the dynamic response of the ankle with its environment is to study its mechanical impedance — a property that describes the torque response to an input ankle motion [2]. Understanding the ankle

This work was supported by the National Science Foundation under Grants 1921046 and 1923760. The authors are with the Polytechnic Institute, Purdue University, West Lafayette, IN 47907, USA (e-mail: garamizo@purdue.edu; lknopp@purdue.edu; rastgaar@purdue.edu).

mechanical impedance during standing and walking is essential for clinical applications, detection of neuromuscular pathologies, stroke rehabilitation, and improvements to effective prosthetic and orthotic devices [3], [4].

The mechanical impedance of the ankle can be described for three degrees-of-freedom (DOF); including rotations in dorsiplantarflexion (DP), inversion-eversion (IE), and medial-lateral (ML) directions [5]. These axes of rotation correspond to motion in the sagittal, frontal, and transverse anatomical planes, respectively. Many techniques for quantifying the ankle impedance have been developed for different scenarios, such as while the ankle is not loaded by the bodyweight [6]–[9], and while the ankle is under load, during standing [10]–[13], walking [14]–[19], and running [20].

Hunter and Kearney studied the non-loaded ankle impedance at various ankle torques [6] and ankle angles [7] while subjects lay in a supine position. They modeled the ankle impedance in the sagittal plane as a 2nd order system (a function of the stiffness, damping, and inertial parameters) and concluded that the stiffness and damping increased with mean ankle torque and angle. Wiess et al. furthered this analysis by studying the differences in ankle impedance while the ankle torque was passive [8], actively held at a constant level [9], and over a range of ankle angles and muscle activation levels [21]. The ankle impedance can be modulated independently of the position of the ankle angle through active contraction of the lower extremity muscles.

Furthermore, the dynamic properties of the ankle during standing have been quantified to investigate the underlying mechanisms of maintaining a stable, upright balance. During quiet standing, the body naturally sways back and forth in the sagittal and frontal planes, using ballistic-like motions to control the individual's center of pressure (COP) [22]–[24]. The contributions from both the intrinsic and reflexive properties of the ankle impedance are necessary to maintain a stable COP and prevent from falling [10]–[12], [25]. When the COP of the foot moves forward towards the anterior direction, increasing the ankle plantarflexion torque, the ankle stiffness in plantarflexion also increased [12], [26]. For all previously stated studies, the subjects stood in a "normal" standing posture, where their feet were positioned side-by-side and parallel to one another. The ankle range of motion in this posture is limited, where the maximum angle is achieved by a slight lean forward or backward [26]. To our knowledge, the ankle mechanical impedance has not been studied for postures other that quiet standing with side-by-side, parallel feet.

These works have quantified the ankle impedance during non-loaded and standing scenarios; however, the majority of these findings are limited to only a single-DOF of the ankle, which potentially overlooks relevant information about the coupling between multiple DOF. Only a few studies have quantified the ankle impedance in the DP and IE DOF. First, the Anklebot, a back-drivable, wearable robot, was used to characterize the multi-directional ankle impedance during nonloaded scenarios. Lee et al. found that the anisotropic ankle impedance in the 2-D space, formed by the DP-IE rotations, resembled a "peanut" shape, where the stiffness in DP was greater than IE, and the maximum stiffness occurred along an axis that was tilted counterclockwise (CCW) from the initial foot coordinate system [27]. Furthermore, they found that the ankle impedance increased in all directions as the lower extremity muscle activity increased [28]. Recently, Nalam et al. quantified the intrinsic ankle impedance in the DP and IE direction during quiet standing [29]. In addition, the authors have also quantified the standing ankle impedance in the DP and IE directions using a 2-DOF vibrating platform [13]. Similar to the non-loaded scenario, the ankle stiffness and damping increased with muscle co-contraction levels during normal standing.

Recently, the time-varying ankle impedance has been quantified during dynamic walking scenarios. The stance phase of the gait cycle can be divided into sub-gait phases, including heel-strike, late-loading response, mid-stance, and terminal stance [30], [31]. The ankle impedance in the sagittal plane has been quantified throughout the stance phase of straight walking [15]–[17], [30] and running [20]. Additionally, Ficanha et al. determined the time-varying ankle impedance during the stance phase of walking in both the sagittal and frontal planes [18], [19], [32], and compared the differences in the impedance during straight walking and performing a turning maneuver [33]. The experimental protocol for estimating the ankle impedance during walking is a very resource-intensive procedure, where each test requires the collection of a few hundred steps from each subject. Often, this requires multiple hours of walking from the subject – which could be very physically intense for a person with a neuromuscular disorder or impairment. Shorter et al. studied the time-varying ankle impedance during walking in patients who had recurrent strokes; however, the test required that the subjects meet specific endurance and walking speed criterion [34].

The purpose of this study was to quantify the multidirectional ankle mechanical impedance while standing in stationary postures that are similar to walking postures. The contributions of this work include: 1) quantify the multidirectional ankle impedance during standing for various standing postures other than quiet standing with side-by-side, parallel feet – which, to the best of our knowledge, has not been determined, 2) explore the changes in ankle impedance during standing, while the ankle angle, torque, and center of pressure are varied, and 3) compare the resulting ankle impedance to previously reported non-loaded, standing, and walking tests about the DP and IE DOF.

II. METHODS

A. Experimental Procedure

1) Subjects

Fifteen able-bodied male subjects with no self-reported history of neuromusculoskeletal pathology or ankle impairment

TABLE I
SUBJECT BIOMETRIC INFORMATION

Metric	Average \pm std
Age (years)	28.0 ± 4.4
Mass (kg)	79.0 ± 11.1
Height (cm)	178.0 ± 7.7
Stance Length (cm)	71.0 ± 3.1
Foot Length (cm)	26.5 ± 1.4

were recruited for this study. All subjects gave written content to participate in the experiment, as approved by the Institutional Review Board (application numbers 423498-10, 371107-9, and 371102-8). An overview of the biometric information is shown on Table I.

2) Apparatus

An instrumented vibrating platform was used to perturb the ankle in all combinations of the sagittal (DP) and frontal (IE) anatomical planes. The vibrating platform contains a force plate module (Kistler 9260AA3) that is fixed to a 2-DOF vibrating platform and is surrounded by motion capture cameras (eight cameras – OptiTrack Prime 17W). The vibrating platform is encompassed by a wooden walkway, allowing the top surface of the force plate and the ground to be level. During an experiment, the subject stood with their right foot placed on the vibrating platform and the resulting ankle torques and angles were measured from the force plate and motion capture cameras, respectively, both with a sampling rate of 350 Hz. A more detailed description of the instrumented platform and methods for measuring the ankle kinetics and kinematics in 2-DOF are found in previous work [35].

3) Protocol

Four stationary standing postures were considered to characterize the mechanical impedance of the ankle, as shown in Fig. 1. Each posture had a different combination of foot center of pressure (COP) and distance between feet (and consequently ankle angle and torque), which were selected to closely resemble stages within the stance phase of the gait cycle [31]. To account for the individual biomechanical differences between subjects, the foot COP and the distance between feet were normalized by the subject foot length and the subject height, respectively. The first posture, defined as Flat Foot (FF), corresponds to the COP that occurs approximately between 3%-12% of the gait cycle, where the foot falls flat on the ground

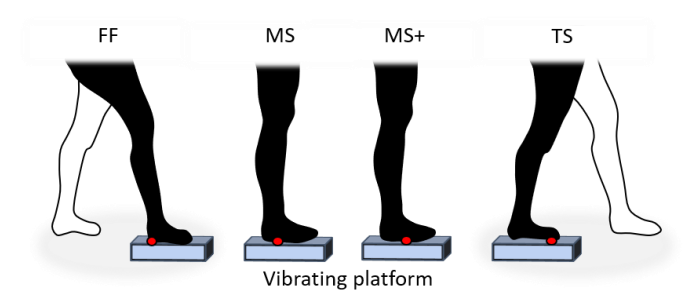


Fig. 1. Four stationary postures that resemble stages within the stance phase of the gait cycle: including Flat Foot (FF), Midstance (MS), Post Midstance (MS+), and Terminal Stance (TS). The red dot indicates the location of the target COP.

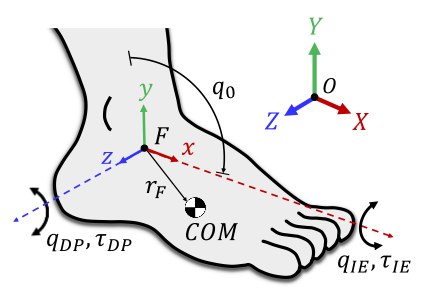


Fig. 3. The foot coordinate frame F located at the ankle center, with the x-axis parallel to the sagittal plane of the foot and the y-axis pointing upwards. The mean ankle angle q_0 is defined by the orientation of the foot with respect to the shank. Any small deviations from q_0 are described by the ankle angle (q) and torque (t) about the x and z axes of rotation.

and begins to stabilize the leg. The subsequent Midstance (MS) and Post Mid-stance (MS+) postures are analogous to the ankle between 12% - 31% of the gait cycle, where the ankle angle decreases and the COP moves forwards. Last, the Terminal Stance (TS) posture resembles the stage in the gait cycle that happens just before the heel starts to rise off the ground. The desired COP location depicted by the red dot in Fig. 1 moves forward in the anterior-posterior direction (x-axis) between the FF and TS postures. The distances between the left and right feet in the anterior-posterior direction (x-axis) for the FF and TS postures were defined to be 20% of the subject's height since there is a strong correlation between height and stride length [36]. However, the distance along the mediolateral direction (z-axis) was self-selected by the subjects.

For all trials, the subjects maintained equal weight distribution between the left and right leg and a constant COP along the anterior-posterior direction. The COP, with respect to the foot length, was calculated using (1), where $\tau_{P,Z}$ are the force plate measurements of torques about the z-axis, which corresponds to motion in DP, $f_{P,Y}$ are the forces acting in the vertical direction, $d_{P,heel}$ is the distance between the heel and the center of the force plate, and L_F is the length of the subject's foot, respectively.

$$COP = \left(\tau_{P,Z}/f_{P,Y} - d_{P.heel}\right)/L_F \tag{1}$$

Real-time visual feedback of the weight distribution between legs, the COP location, and the target COP location were provided for each posture. The target COP locations were defined to be 27%, 41%, 53%, and 67% of the subject's foot length, starting from the heel, for the FF, MS, MS+, and TS postures, respectively.

During each trial, the subject stood in one of four postures while ground perturbations were applied to the ankle. The perturbations were randomly selected pulse trains (0.9 - 1.1 s) that varied in axis of rotation $(0^{\circ} - 360^{\circ})$, frequency (5 - 33 Hz), however, perturbations data with frequency above 25 Hz were discarded due to lower signal to noise ratio), and pause time period (0.9 - 1.1 s) in between pulses. The purpose of the pause time of the vibrating platform was for the subjects to recover a natural stance after the previous ground perturbation. The average peak-to-peak angle was 1.9° for frequencies under 10 Hz, then decreased to 0.9° at 25 Hz. The duration of each trial was 30 seconds, and there was a required rest period between

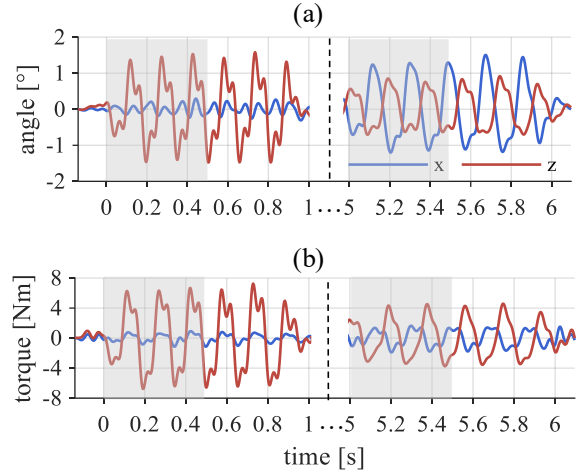


Fig. 2. Two sample pulse train perturbations with the (a) ankle angle and (b) ankle torque. The first example perturbation (to the left of the black dashed line) was applied along DP with a frequency of 6.2 Hz, while the second example perturbation (to the right of dashed lined) was applied along (DE)-(PI) (from dorsi-eversion to plantar-inversion) with a 5.3 Hz frequency. The gray box shows the selected analysis window (0.5 s), starting from the beginning of the pulse train. The DP and IE anatomical axes are described by the x and y axes, respectively.

each trial of at least one minute. Each standing posture was repeated three times, for a total of 12 trials. There was, on average, 36.5 different perturbations per subject per posture. To maintain consistency throughout all trials, the foot outline was drawn on the vibrating platform so that the foot was positioned in the same location for every trial.

B. Multi-Directional Ankle Impedance Model

The numerical derivatives of the kinematic data were calculated using a Savitzky-Golay filter with a 15-sample window and 5th order polynomial. All kinematic and kinetic data measurements were lowpass filtered (cutoff 25 Hz, 5th order Butterworth filter) to reduce the effects of high-frequency sensor noise. Additionally, to remove the natural sway of the body during the perturbation, the ankle angle and torque were detrended by a best-fit cubic curve within a time window starting at the onset of the perturbation and lasting 0.5 seconds. The samples before this window were not used because external perturbations are necessary to separate the intrinsic ankle dynamics from the reflexive dynamics in the presence of sensor noise [1]. Samples after the window were also discarded because, generally, subjects engaged their ankle to regain balance, causing large deviations in the ankle angle and torque.

An example of two pulse train perturbations, including the resulting ankle angle (q_{IE},q_{DP}) , ankle torque (τ_{IE},τ_{DP}) , and the window for impedance estimation are shown in Fig. 3. The red and blue lines represent the ankle rotation and torque about the x and z axes of rotation, and the gray box represents the window of data that was selected from each pulse train to estimate the ankle impedance. All measurements about the anatomical External-Internal (EI), or y axis, was assumed to be small because the vibrating platform does not apply perturbations in the y axis, and their impact on the ankle impedance estimation was not considered for this study.

The multi-directional ankle impedance was estimated as in previous work by the authors [37]. In this method, the muscles, tendons, and ligaments in the lower leg contribute as impedance components acting along with arbitrary motion directions. However, using small-angle and linearity assumptions, the combined effect of all the impedance components is briefly represented by three symmetric matrices, characterizing the stiffness, damping, and ankle inertia components. For the complete derivation of these equations, please refer to [37]. These matrices map the ankle angular displacement, velocity, and acceleration $(q, \dot{q}, \ddot{q}, respectively)$ to the ankle torques (τ) , noting that the notation for all boldened variables represent a vector and non-boldened variables represent magnitude. The ankle kinematic and torque variables in (2) are \mathbb{R}^3 vectors that contain elements for the IE, EI, and DP anatomical axes. The ankle impedance torque is described as:

$$\boldsymbol{\tau_{imp}}(\boldsymbol{q}, \dot{\boldsymbol{q}}, \ddot{\boldsymbol{q}}) = \begin{bmatrix} K_x & 0 & K_{xz} \\ 0 & 0 & 0 \\ K_{xz} & 0 & K_z \end{bmatrix} \boldsymbol{q} + \begin{bmatrix} B_x & 0 & B_{xz} \\ 0 & 0 & 0 \\ B_{xz} & 0 & B_z \end{bmatrix} \dot{\boldsymbol{q}} + \begin{bmatrix} J_x & 0 & J_{xz} \\ 0 & 0 & 0 \\ J_{xz} & 0 & J_z \end{bmatrix} \ddot{\boldsymbol{q}}$$

$$= \begin{bmatrix} J_x & 0 & J_{xz} \\ 0 & 0 & 0 \\ J_{xz} & 0 & J_z \end{bmatrix} \ddot{\boldsymbol{q}}$$
(2)

described as a function of its stiffness (K_x, K_z, K_{xz}) , damping (B_x, B_z, B_{xz}) , and ankle inertia (J_x, J_z, J_{xz}) properties. The coupling behavior between the IE and DP DOF was represented by K_{xz} , B_{xz} , and J_{xz} . Note that this ankle inertia is not the same as the foot inertia. Rather than representing the mass distribution of the foot, it represents the mass of the muscle tissues that move when ankle joint moves, and possibly also describes high-order dynamics.

To quantify the anisotropic characteristics of the ankle impedance, the stiffness, damping, and ankle inertia components are evaluated for an angle disturbance of magnitude $q \in \mathbb{R}$ and an axis of rotation parameterized by an angular displacement direction φ :

$$\mathbf{q} = q \cdot [\sin(\varphi) \quad 0 \quad \cos(\varphi)]^T \tag{3}$$

The variable φ spans all angles in the DP-IE space, taking the value of 0°, 90°, 180°, and 270°, for dorsiflexion, inversion, plantarflexion, and eversion, respectively. Summarizing the analytical results of [37], the net ankle stiffness, damping, and ankle inertia are

$$K(\varphi) = \frac{K_z - K_x}{2} \cos 2\varphi + \frac{K_z + K_x}{2} + K_{xz} \sin 2\varphi$$
 (4)

$$B(\varphi) = \frac{B_z - B_x}{2} \cos 2\varphi + \frac{B_z + B_x}{2} + B_{xz} \sin 2\varphi$$
 (5)

$$J(\varphi) = \frac{J_z - J_x}{2} \cos 2\varphi + \frac{J_z + J_x}{2} + J_{xz} \sin 2\varphi$$
 (6)

This resulting ankle impedance model was added into the equation of motion of the lower leg system, which considered the foot as a single rigid body. The equation of motion of the lower leg system is derived from the angular momentum of the foot, L_F , around the ankle center.

$$\sum_{F} \boldsymbol{\tau} = \frac{d\boldsymbol{L}_{F}}{dt}$$

$$\tau + r_F \times mg + \tau_Z(q, \dot{q}, \ddot{q}) = \frac{d(l\omega + r_F \times m\dot{s}_0)}{dt}$$

$$= l\dot{\omega} + \omega \times (l\omega) + r_F \times m\ddot{s}_0 + (\mathbf{0} + \omega \times r_F) \times m\dot{s}_0$$

$$\tau = l\dot{\omega} + \omega \times (l\omega) + r_F \times m(\ddot{s}_0 - g) + (\omega \times r_F) \times m\dot{s} + \tau_{imp}(q, \dot{q}, \ddot{q})$$
(7)

Each variable is described as:

au the external torque acting on the ankle

 L_F the angular momentum of the foot

 r_F the vector from foot coordinate to COM

m the foot mass

I the moment of inertia tensor of the foot

 ω the foot angular velocity

 $\dot{\boldsymbol{\omega}}$ the foot angular acceleration

 \dot{s}_0 the foot linear velocity, i.e. $\dot{s}_0 = \dot{s} + \omega \times r$

 $\ddot{\mathbf{s}}_{\mathbf{0}}$ the foot linear acceleration, i.e.

$$\ddot{\mathbf{s}}_0 = \ddot{\mathbf{s}} + \dot{\boldsymbol{\omega}} \times \mathbf{r} + \boldsymbol{\omega} \times (\boldsymbol{\omega} \times \mathbf{r}).$$

Differently from [37], where (7) is linearized and the ankle impedance and foot inertia parameters are estimated via linear least-squares, in this work, the unknown parameters are estimated directly from the nonlinear equation (MATLAB's *fmincon* function, interior-point algorithm [38]). This adaptation was necessary because the cyclic perturbation used in this experiment creates high collinearity between the plate, shank, and foot motions. Even though the collinearity would not hinder the torque prediction, it could bias the impedance parameter estimates [39].

The nonlinear regression problem was solved defining the mean squared error of (7) as the cost function. The cost function evaluates the torque prediction error as a function of a vector of unknown variables (i.e., the ankle impedance and foot inertia coefficients). Given an initial estimate and boundaries for the unknown variables, the nonlinear solver minimizes the torque prediction error. The initial estimates were selected as values previously reported in the field. And boundaries were added to represent physical limitations, such as constraining $K(\varphi)$, $B(\varphi)$, and $J(\varphi)$ (from (4-6)) to be greater than or equal to zero, assuming the ankle resembles a stable $2^{\rm nd}$ order system. These boundaries reduced the region of search and helped the solver to find a better fit for the cost function.

Last, to solve for the impedance coefficients of each posture, the data from the three repeated 30-second trials were combined. Next, each pulse train perturbation was individually selected using a window that started at the onset of the pulse train and had a length of 0.5 seconds. The net ankle impedance for each posture was determined by substituting the coefficients into (4-6) to calculate $K(\varphi)$, $B(\varphi)$, and $J(\varphi)$ for all angle directions φ and were presented in the form of polar plots.

C. Statistical Methods

To evaluate the accuracy of the ankle impedance model, the percent Variance Accounted For (%VAF) was determined using the reconstructed external torque ($\hat{\tau}$) and the measured torque (τ). To determine the %VAF throughout the DP-IE space, the reconstructed torque and measured torque parameters were projected to all angle directions φ . The %VAF was

determined for each posture and was presented in polar coordinates.

$$\%VAF(\varphi) = 1 - \frac{var(\boldsymbol{u}(\varphi)^{T}(\boldsymbol{\tau} - \hat{\boldsymbol{\tau}}))}{var(\boldsymbol{u}(\varphi)^{T}\boldsymbol{\tau})}$$
(8)

where $\mathbf{u}(\varphi) = [\sin(\varphi) \quad 0 \quad \cos(\varphi)]^T$ is the unit vector that defines the axis of rotation of the ankle angle. Moreover, to demonstrate the generalization of the impedance model, the perturbations were randomly divided into training and testing sets containing 75% and 25% of the perturbations, respectively. For the calculation of the VAF, the impedance model was estimated using the training set, and the torque was reconstructed with the testing set.

Additionally, a series of Analysis of Variance (ANOVA) tests were performed to compare the ankle impedance estimated for different standing postures in this study and compare these results to previous work. First, this study compared the changes in the multi-directional ankle impedance throughout the four standing postures. A one-way repeated measures ANOVA with a post hoc paired t-test with Bonferroni corrections were used to compare different ankle angle, torque, and impedance parameters across the four postures. This within-subject analysis is designed to account for data from the same subjects in all groups [40]. For the impedance, each of the coefficients $(K_x, K_z, K_{xz}, B_x, B_z, B_{xz}, J_x, J_z, J_{xz})$ were evaluated individually, where the independent groups were defined as the four postures (FF, MS, MS+, and TS), and the null hypothesis states that the means are equal. The statistical significance for each coefficient, using the one-way Repeated Measures ANOVA, were judged with an experiment-wise (EW) significance level of $\alpha_{EW} = 0.05$. To reduce Type I error, the Bonferroni post hoc analysis further reduced the per-comparison (PC) alpha to $\alpha_{PC} = 0.0083$, determined by dividing α_{EW} by the total number of post hoc comparisons performed.

Last, this study examined the similarities and differences between the ankle impedance during varied standing postures with previous findings that determined the ankle impedance during non-loaded and walking scenarios. For these tests, a one-way ANOVA was selected to compare the ankle impedance with similar ankle angles and torques during loaded and non-loaded conditions. Similar to the repeated measures ANOVA, the critical value, F, was determined using an experiment-wise (EW) significance level of $\alpha_{EW}=0.05$ for all tests, and the null hypothesis states that the mean values are equal.

III. RESULTS

A. Ankle Torque and Angle during Standing

During each experiment, the subjects stood in one of the four standing postures and were required to maintain their COP within the desired target region. Each posture varied the ankle angle and torque to achieve the target COP location. The resulting subject average COP locations in the anterior-posterior direction were $27.5\% \pm 1.6\%$, $41.4\% \pm 1.3\%$, $53.7\% \pm 1.9\%$, $67.0\% \pm 2.9\%$ for the FF, MS, MS+, and TS postures, respectively. As the foot COP moved forward, the ankle torques in the DP direction all statistically differed from one another $(F_{3,42} = 839.7, p < 0.05)$, with increasing average values of 0.06 ± 0.04 Nm/kg, 0.25 ± 0.03 Nm/kg, 0.40 ± 0.04 Nm/kg, and 0.60 ± 0.05 Nm/kg for the FF, MS, MS+, and TS postures,

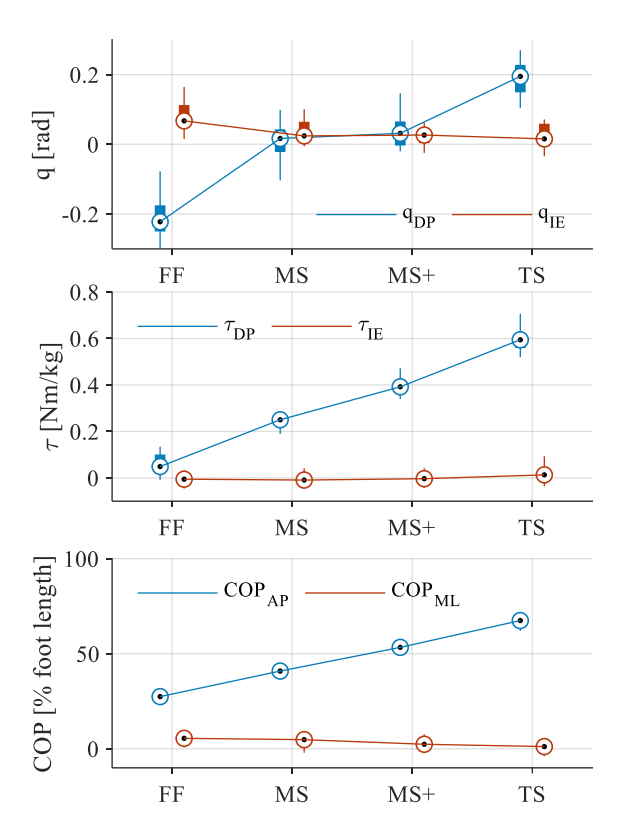


Fig. 4. Box plots of mean angles, torques, and COP between subjects separated by different stationary postures. In this plot, the maximum, third quartile, median, first quartile, and the minimum, are shown by the top of the vertical line, top of the box, circle, bottom of box, and bottom of vertical line, respectively. The sample size was the number of subjects.

respectively. Furthermore, the ankle torques in the IE direction also showed an increasing trend that ranged on average between -0.005 ± 0.02 Nm/kg to 0.02 ± 0.04 Nm/kg across the four postures. Using repeated measures ANOVA, there were statistical differences ($F_{3,42} = 7.5$, p > 0.05); however the posthoc pairwise comparisons showed that there were no statistical difference between the FF and MS (p = 0.49), the FF and MS+ (p = 0.22), the FF and TS (p = 0.02), and the MS and MS+ (p = 0.01) postures. Fig. 4 shows the boxplot of the ankle torque in DP (z) and IE (z) across each posture, which was normalized by the subjects' masses. The negative angle and negative torque describe ankle motion in plantarflexion and eversion, respectively.

Additionally, the average ankle angles across subjects are also presented in Fig 4. Similar to the torque, the ankle angles in DP were statistically different ($F_{3,42}$ = 133.8, p < 0.05) for each posture, with the exception of the MS and MS+ postures (p = 0.05, after Bonferroni correction), with average values of -0.2 ± 0.08 rad, 0.01 ± 0.04 rad, 0.04 ± 0.06 rad, and 0.18 ± 0.05 rad for FF, MS, MS+, and TS postures, respectively. Notably, for the MS and MS+ postures, the average ankle angle did not show a statistical difference, while the ankle torque in these postures did. The ankle angles in IE decreased, with only the first posture showing a significant difference ($F_{3,42}$ = 25.8, p < 0.05) from the other three postures after the pairwise Bonferroni correction. The average ankle angles ranged from 0.07 ± 0.04

TABLE II AVERAGE \pm STD OF THE IMPEDANCE COEFFICIENT ESTIMATES ALONG THE X AND Z AXES OF ROTATION FOR 15 SUBJECTS.

	FF	MS	MS+	TS		
Stiffness [Nm/rad/kg]						
K_x	0.81 ± 0.19	0.94 ± 0.27	1.10 ± 0.35	1.10 ± 0.40		
K_{xz}	0.09 ± 0.06	0.05 ± 0.17	0.11 ± 0.23	0.46 ± 0.31		
K_z	0.91 ± 0.26	2.50 ± 0.37	3.71 ± 0.61	4.25 ± 0.84		
Damping [Nms/rad/kg×10 ⁻³]						
B_x	0.95 ± 0.64	2.33 ± 1.80	3.54 ± 1.87	5.77 ± 2.17		
\boldsymbol{B}_{xz}	1.02 ± 0.95	0.28 ± 1.47	0.66 ± 1.98	0.66 ± 2.26		
B_z	4.60 ± 2.63	6.70 ± 4.42	7.93 ± 4.77	10.57 ± 4.63		

rad to 0.0014 ± 0.04 rad from the FF to TS postures, respectively.

Ideally, the ankle torque, ankle angle, and COP location would remain constant across the trial in order characterize the ankle impedance for the corresponding posture. However, there were deviations from these average values (Fig. 4) due to the perturbations or from the subject's loss of balance. To evaluate these deviations, the average was removed within each set of subject and posture trials, and the standard deviation was calculated across all the measurements (combining data from multiple subjects and postures). The standard deviation of the COP_{AP} , COP_{ML} , τ_{DP} , τ_{IE} , q_{DP} , q_{IE} was 3.8% foot length, 3.4% foot length, 31.2×10^{-3} Nm/kg, 33.0×10^{-3} Nm/kg, 23.0×10^{-3} rad, and 24.6×10^{-3} rad, respectively.

B. Multi-directional Ankle Impedance

The ankle impedance varied across different standing postures where the COP of the foot was moved forward. Table II shows the average impedance parameters across the population. As expected, the average ankle stiffness and damping were higher in the DP direction compared to the IE and the coupled coefficients. Additionally, the stiffness and damping in the DP direction increased as the COP moved forward.

The repeated measures (within-subject) ANOVA comparing the ankle impedance (Table II) across standing posture showed significant differences for all coefficients (p < 0.05), except B_{xz} (F_{3,42} = 0.59, p > 0.10). The stiffness coefficient in K_z direction increased significantly across all postures (p < 0.05), with the average stiffness increasing by a factor of 4.5. However, the average stiffness in the K_x direction increased at a smaller factor of 1.4, only showing a statistical difference between the FF and MS posture (p < 0.05) and the FF and MS+ postures (p < 0.05).

The average damping in the B_z direction showed significant differences (p < 0.05) between the FF and MS+, FF and TS, MS and MS+, and MS and TS postures, increasing by a factor of 2.3. Similarly, the B_x damping direction had significant differences (p < 0.05) between the FF and MS+, FF and TS, and MS and TS postures, increasing by a factor of 6.6. No statistical differences were found between the FF and MS (p > 0.009) and MS+ and TS (p > 0.01) postures for both directions while using the Bonferroni correction factor.

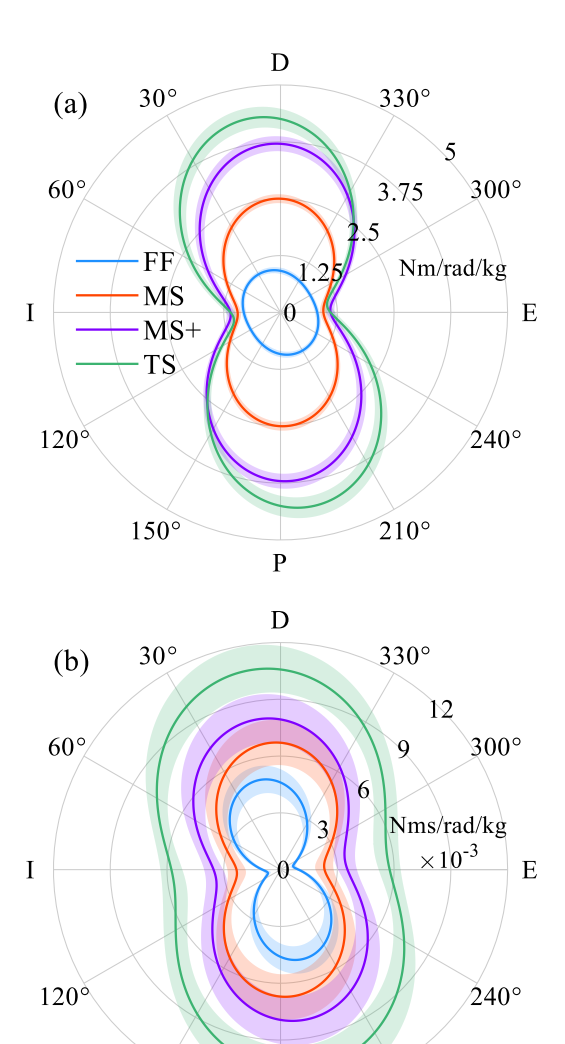


Fig. 5. Multi-directional ankle impedance across the four standing postures; including the a) stiffness and b) damping parameters for all angle directions, φ , in the DP-IE space. The φ angles 0° , 90° , 180° , and 270° correspond to dorsiflexion, inversion, plantarflexion, and eversion of the ankle, respectively. The solid blue, orange, purple, and green lines represent the average impedance across 15 subjects for the FF, MS, MS+, and TS standing postures, respectively. The shaded region is the standard error across subjects.

P

210°

150°

Using (4-6), the variation of ankle impedance depending on the direction was characterized for angles (φ) ranging from 0° to 179°, with an increment of 1°. The polar plots presented in Fig. 5 describe the average ankle stiffness (a) and damping (b) of the ankle impedance estimation in the DP-IE space, where the blue, orange, purple, and green lines correspond to the FF, MS, MS+, and TS standing postures, respectively. The solid line shows the average curve across all subjects, and the shaded region is the standard error. The magnitudes of each coefficient were dependent on the standing posture and on the angle direction φ ; were the impedance was greater in DP than IE, resulting in a distinctive "peanut" shape.

The directions of the major axes (Fig. 5), which display the largest stiffness and damping magnitudes, were calculated for

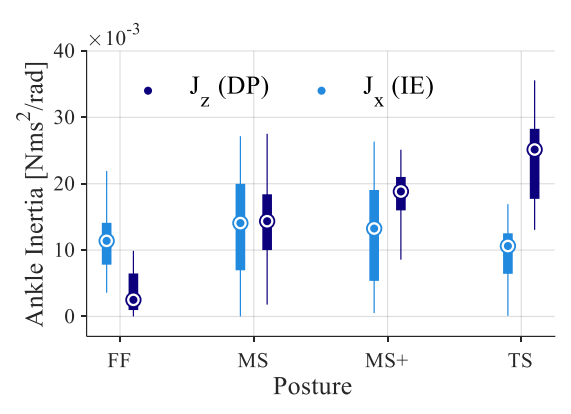


Fig. 6. Boxplot of ankle inertia across subjects for FF, MS, MS+, and TS poses in the DP (dark blue) and IE (light blue) directions.

each posture. The maximum stiffness and damping were along with dorsi-inversion and plantar-eversion ankle rotations. The minor axis was defined as the amplitude of the impedance rotated 90° from the major axes.

The average foot moment of the inertia I, mass m, and center of mass r_F across all trials were, respectively, $diag([0.4 \pm 0.6, 1.2 \pm 2.2, 9.9 \pm 5.9]) \times 10^{-3} \,\mathrm{kg.m^2}$, $1.784 \pm 0.077 \,\mathrm{kg}$, and $[44.5 \pm 8.7, -17.5 \pm 9.0, -0.0 \pm 6.6]^{\mathrm{T}} \times 10^{-3} \,\mathrm{m}$, where diag(.) represents the vector to diagonal matrix operator. On the other hand, the average ankle inertia, J_x , J_{xz} , and J_z (per Equation (6)), were $12.0 \pm 7.2 \times 10^{-3} \,\mathrm{Nm/rad/s^2}$, $-0.5 \pm 3.9 \times 10^{-3} \,\mathrm{Nm/rad/s^2}$, and $14.9 \pm 9.4 \times 10^{-3} \,\mathrm{Nm/rad/s^2}$, respectively (Fig. 6). The repeated-measures ANOVA with Bonferroni corrections determined a significant difference (p < 0.05) between all postures in the DP direction, with an exception between the MS+ and TS postures (p = 0.015, with post hoc corrected p-value of 0.0083). There were no statistical differences determined across all postures for the ankle inertia in the IE direction (F_{3,42} = 0.26, p > 0.50).

Last, an average %VAF of $81.6 \pm 6.9\%$, $89.6 \pm 5.2\%$, $91.1 \pm 5.0\%$, and $83.5 \pm 9.2\%$ was determined for the FF, MS, MS+, and TS postures, respectively. Fig. 7 shows that the %VAF for each angle directions ($\varphi = 0^{\circ}$ to 359°) varied slightly depending

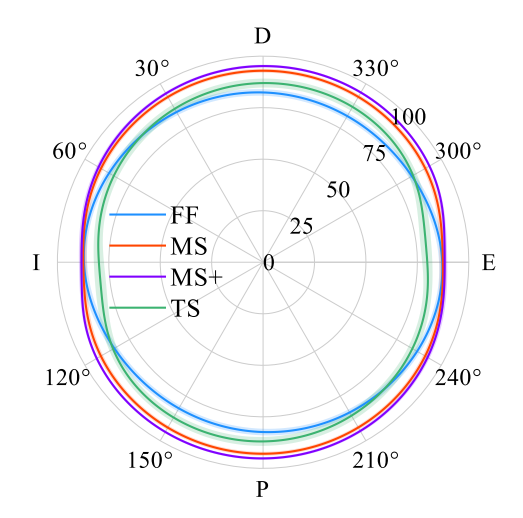


Fig. 5. %VAF \pm standard error across subjects for the measured ankle torque and reconstructed ankle torque from the impedance model. The results are presented in polar coordinates for each angle direction φ .

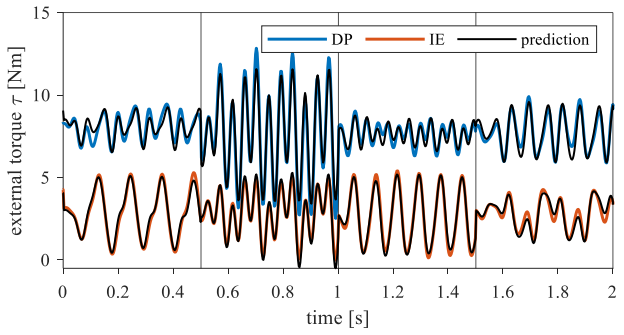


Fig. 8. External torque measured by the force plate and the predicted torque (left and right hand-side of Equation (7), respectively) for a representative subject at the FF posture. Different sections of the perturbation are separated by the vertical black lines.

on the posture and direction φ . The high %VAF across subjects shows that the characterized impedance model was able to predict the resultant ankle torque with considerable accuracy (Fig. 8). Interestingly, we noticed larger torque residuals from high-frequency perturbations and perturbations with axes of rotation near the IE axis of the ankle.

IV. DISCUSSION

In this study, we describe the multi-directional ankle impedance during standing with four postures. The stationary standing postures were selected to resemble instances within the subphases of the stance phase of the gait cycle (GC), where the ankle angles and torques are adjusted accordingly. The subphases of interest included the moment after heel strike, during the loading response (2% - 12% GC), throughout the mid-stance (12% - 31% GC), and during terminal stance (31% - 50% GC) before the heel comes off the ground [31].

A. Impedance Characterization

The resulting ankle impedance (Fig. 5) shows that the stiffness and damping varied depending on the ankle angle and COP during each standing posture. As the foot COP moved forward along the foot longitudinal axis, the ankle angle and ankle torque increased (Fig. 4). The magnitude of the impedance parameters was, in general, much greater in the DP direction than in the IE direction, creating a pinched, "peanut" shaped polar plot. Lee et al. first presented a similar shape for the multi-directional ankle stiffness determined while the ankle was not loaded [27], [28]. They did not find significant changes in B_x with varying levels of dorsiflexion and plantarflexion muscle activity and with a neutral ankle angle [28]. In contrast, we found significant differences in B_x (p < 0.05) between the FF and MS+, FF and TS, and MS and TS postures. No statistical differences were found between the FF and MS (p > 0.009) and MS+ and TS (p > 0.01) postures for both directions while using the Bonferroni correction factor. These results suggest that B_r is more sensitive to DP ankle angle deviations than to muscle activations, within our testing conditions.

The directional characteristics of the ankle stiffness and damping were tested with a one-sample t-test by verifying whether their major axes are significantly different than zero (DP axis) among the subjects. As seen in Fig. 5a and Table III, the major axis of the stiffness was significantly different from

the DP axis for the postures FF (t(14) = 4.75, p < 0.05) and TS (t(14) = 5.94, p < 0.05), with average values of $31.7^{\circ} \pm 25.8^{\circ}$ and $8.5^{\circ} \pm 5.6^{\circ}$, respectively. The stiffness curves with the major axes that had the smallest deviation from DP were found during the MS $(1.5^{\circ} \pm 7.2^{\circ})$ and MS+ $(2.7^{\circ} \pm 5.5^{\circ})$ postures. Similarly, previous work that characterized the non-loaded, multi-directional ankle impedance found that the major axes of the stiffness were tilted from the DP direction, ranging between $2.8^{\circ} \pm 5.4^{\circ}$ to $5.2^{\circ} \pm 5.4^{\circ}$ when the muscle activity was small [28]. These previous findings also determined the ankle impedance while the SOL muscles, responsible for ankle plantarflexion, were contracted to 50% of the subjects' Maximum Voluntary Contraction (MVC) and found that the stiffness major axes increased to an average angle direction of $\varphi = 13.2^{\circ} \pm 9.1^{\circ}$. Interestingly, during the TS posture – where the ankle torque and muscle activity of the SOL were greatest – the major axes of the stiffness was shifted to $8.3^{\circ} \pm 5.2^{\circ}$, similar to the results presented in [28].

The multi-directional ankle damping (Fig. 5b and Table III), which has not been previously determined for the standing postures, showed major axes significantly different than zero (t(14) = 3.29, p < 0.01) only for the FF posture (17.5° ± 20.6°). Both the stiffness and damping during FF have major axes in the first and third quadrants of φ . During the FF, the right foot leads the left foot, creating a base of support that has structural stability along with the second and fourth quadrants. We hypothesize that the ankle impedance can improve body stability during the right heel strike by decreasing the ankle impedance along the stable ankle axis – the second and fourth quadrants of φ – deflecting motions along the unstable ankle directions. Further gait trials will be needed to test this hypothesis.

The joints within the ankle do not rotate about axes that are aligned with the anatomical axes, explaining why the major and minor axes are tilted [5]. However, based on these observations, the direction and magnitude of the major axes could also be dependent on the amount of muscle activity, ankle angle, and ankle torque generated for a given posture. Future work can study the function and significance of these tilted major axes during activities of daily living and its implications in the design of prosthesis controllers.

The characterized foot inertia was larger than expected, with a mass 58% larger than the average foot mass of the male population [41]. The foot inertia parameters are less accurate than the other impedance parameters considering that the moment of inertia of the instrumental apparatus alone is more than ten times larger than of the foot. Due to their highly correlated motions, it is possible that the foot inertia estimates were biased by residuals of the experimental apparatus' inertia that were not sufficiently reduced. For more accurate measurements of the foot inertia, we believe other direct approaches, such as cadaver studies or water immersion techniques, could be used [42].

In this work, the foot inertia was differentiated from the ankle inertia. In the former, the reaction torque is proportional to the foot angular acceleration, $\dot{\omega}$ (Equation (7)), while in the later, the reaction torque is proportional to the joint angle acceleration, \ddot{q} (Equation (6)). This ankle inertia parameter models the mass of small tendons, ligaments, and muscles that move when the ankle angle changes. This parameter could also

TABLE III
ANKLE STIFFNESS AND DAMPING ALONG MAJOR AND
MINOR AXIS DIRECTIONS

	Direction of Major axes	Amplitude of Major Axes	Amplitude of Minor Axis
		Stiffness	
	[degrees]	[Nm/rad/kg]	[Nm/rad/kg]
FF	31.7 ± 25.8	1.08 ± 0.31	0.72 ± 0.23
MS	1.5 ± 7.2	2.60 ± 0.48	0.97 ± 0.32
MS+	2.7 ± 5.5	3.83 ± 0.76	1.10 ± 0.36
TS	8.5 ± 5.6	4.40 ± 0.94	1.03 ± 0.34
		Damping	
	[degrees]	[Nms/rad/kg] ×10 ⁻³	[Nms/rad/kg] ×10 ⁻³
FF	17.5 ± 20.6	5.31 ± 3.55	0.37 ± 0.52
MS	-14.2 ± 42.8	7.81 ± 5.03	1.35 ± 1.47
MS+	5.2 ± 34.1	9.70 ± 5.11	2.31 ± 2.23
TS	7.1 ± 35.7	12.17 ± 5.01	4.42 ± 2.50

be affected by high-frequency components of the impedance due to high-order dynamics [43]. The ankle inertia remained small, with values less than 40 g.m² across all subjects for the DP and IE directions. While the IE inertia remained relatively constant, as expected from an inertial property, the DP stiffness changed between postures. It is possible that the effect of the ankle inertia is relatively small for the perturbations used in this experiment, which, combined with the measurement noise, could cause a bias in the inertial parameters. Other sources of parameter bias include unmodeled high-order dynamics, such as not including antiresonances in the impedance model [43] and muscle reflex contributions [44], or correlated noise among the predictors of the impedance regression model (e.g., ankle velocity and acceleration). A possible strategy to reduce these effects in the impedance characterization, and that will be experimented in the future, is to account for non-linear dynamics in the model and to model the noise correlation between samples and predictors via Expectation Maximization algorithms [45].

Last, the %VAF determined for all angle directions φ (averaged across all subjects and postures) was $86.4 \pm 7.7\%$, showing that the impedance model presented was able to account for most of the measured torque. The %VAF, in all directions, was higher in the MS and MS+ postures and slightly lower in the FF and TS postures (Fig. 7). This difference in torque prediction accuracy may be related to some subjects having a less stable stance in the FF and TS postures, causing the generation of additional torques around the ankle due to reflex muscle activity. In turn, this may introduce internal torques that were not accounted for in the impedance model.

Furthermore, for all postures, the %VAF was lower along the IE axis. The vibration platform used in this study can apply angle perturbations in similar magnitudes in both DP and IE; however, it applies more torque in the DP than in the IE DOF [35]. It is possible that the later DOF was not perturbed with enough energy, or the noise present in the measurement system contributed to the decrease in %VAF. Further improvements to the %VAF might be achieved by making changes to the experimental protocol and modeling techniques. For example, the impedance model could be extended to include reflex contributions [46] in both ankle DOF, or nonlinear effects from

small ankle angle and torques deviations [37], and muscle cocontractions [9], [28] that occurred within trials.

B. Comparison to Non-Loaded Ankle Impedance

One of the objectives of this study was to determine the similarities and differences between the non-loaded and standing ankle impedance when the ankle has varied angles and torques. Early work by Weiss et al. characterized the ankle impedance in the sagittal plane while the subjects were in a supine position [9]. During that test, the ankle impedance of five subjects was characterized while the ankle angle was positioned at ten different mean angles, covering its full range of motion approximately between -0.94 rad to 0.21 rad. At each ankle position, six different levels of active ankle plantarflexion torque were measured, varying from 10% to 50% MVC. They reported the stiffness as a linear function of ankle torque, for each subject and for each mean ankle angle. To compare our results during standing, we interpolated the average DP ankle torque and angle from our subjects for each posture (Fig. 4) in each of the subject stiffness models to compare the corresponding ankle stiffness. The results of the ankle stiffness in the sagittal plane from Weiss et al. are presented in Fig. 9 alongside the ankle stiffness results for each posture in this study.

Surprisingly, the ankle stiffness for the supine test was greater than the corresponding standing test for all four combinations of ankle angle and torque. A one-way ANOVA was used to compare the two studies and determined that the mean values were statistically different (p < 0.05) for all four postures. Note that the ankle stiffness has been shown to be nonlinear to the magnitude of the angle perturbations, assuming lower stiffness for larger angle magnitudes [7]. However, the supine test used larger angle perturbations (5.2° peak-to-peak) than the standing test (1.9° peak-to-peak) but still resulted in larger ankle stiffness. This difference could be explained by different force loading conditions across the ankle, or different muscle co-contraction activities [9], [28], [37]. During the supine test, the experiment was designed to generate isometric contractions of a single muscle group and to have minimal effects from antagonistic muscles. In contrast, in the standing

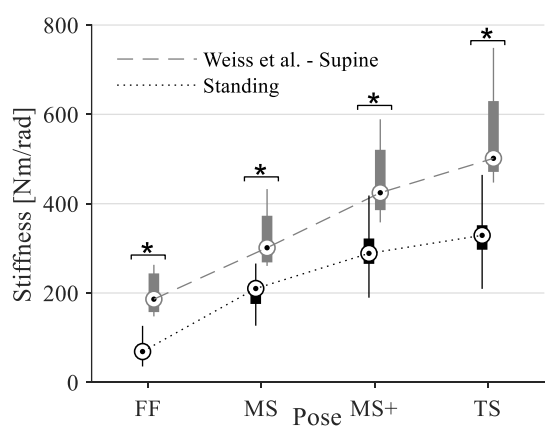


Fig. 6. Comparison of the ankle stiffness in the sagittal plane during standing in four postures to non-loaded ankle with varied mean ankle angle and ankle torques, presented in [9]. One-way ANOVA determined statistical differences, where * denotes p < 0.001.

investigation, there were no limitations on how the muscles were contracted. Finally, the stiffness increased at a similar rate in both experiments, suggesting that the ankle stiffness changed by the same amount depending on the angle and torque generated; however, the average stiffness of the ankle during the supine test was greater than the stiffness during standing by approximately 178.5 Nm/rad.

C. Comparison to Quiet Standing

During quiet, normal standing, where the feet were placed side-by-side, the ankle stiffness and damping vary continuously with sway. Previous work by Loram et al. and Casadio et al. estimated that the ankle stiffness in the DP direction during standing had average values of 297 \pm 68.8 Nm/rad and 366.7 \pm 99.6 Nm/rad, respectively, for two different quiet standing tests [10], [11]. The corresponding average ankle impedance in DP for our study during the MS and MS+ postures, which also had feet positioned side-by-side, ranged between 198.5 ± 36.8 Nm/rad and 292.9 ± 58.3 Nm/rad for stiffness, respectively. The damping and ankle inertial parameters of the ankle were not reported in previous work. Moreover, we have previously quantified the ankle impedance in the IE direction during standing and found comparable ankle impedance to this study [13]. However, the multi-directional impedance was not reported.

D. Comparison to Dynamic Walking

The mechanical impedance during dynamic tasks, such as during walking or running, showed time-varying characteristics throughout the stages within the gait cycle [30]. Depending on the task, the ankle must be able to absorb the shock from the ground impact, generate power to propel the body mass forward, and adjust to unexpected changes in a maneuver. The ankle impedance is dependent on the selected gait speed and the direction of the maneuver. Because of this, it was not possible to make a direct comparison between our results for standing and previous studies. However, we were able to determine similar characteristics, described as follows.

First, during the beginning of the stance phase, at approximately 0% to 12% of the gait cycle, the heel contacts the ground, the ankle angle increases in plantarflexion, and the ankle begins to accept the bodyweight [31]. Lee et al. studied the ankle impedance just before and after heel-strike and determined that the stiffness and damping parameters started to increase just before heel-strike, and then considerably increased just after heel-strike in both the DP and IE directions [16]. They found that the stiffness in IE was greater than or equal to the stiffness in DP just after heel-strike. Interestingly, we saw a similar trend during the FF posture, as described in Table II and Fig. 5a (blue curve). In this posture, the stiffness in IE (0.81 \pm 0.19 Nm/rad/kg) was the closest to the stiffness in DP (0.91 \pm 0.26 Nm/rad/kg). Additionally, our results reported the smallest stiffness and damping for the FF posture, when compared to the other three postures.

Between 12% to 31% of the gait cycle, the COP moves towards the anterior direction of the foot [31], and the stiffness and damping properties in the sagittal plane increases [15]. Rouse et al. reported that the ankle stiffness increased linearly between 1.5 Nm/rad/kg to 6.5 Nm/rad/kg while the ankle damping, although small, had an increasing trend up to $30 \times 10^{-}$

 3 Nms/rad/kg [15]. Ficanha et. al. [18] reported DP stiffness ranges of 1.7 ± 1.1 Nm/rad/kg to 4.4 ± 1.3 Nm/rad/kg, and DP damping ranges of $18\pm26\times10^{-3}$ Nms/rad/kg to $50\pm29\times10^{-3}$ Nms/rad/kg. The gait phase studied by Rouse et al. and Ficanha et al. have comparable trends to the MS, MS+, and TS postures reported in this study. In this present study, the ankle DP stiffness significantly increased from 2.50 ± 0.37 Nm/rad/kg to 4.25 ± 0.84 Nm/rad/kg, which falls within the range of stiffness during dynamic walking. Furthermore, the DP damping was less than the average during walking but similarly showed increasing trends, ranging $6.70\pm4.42\times10^{-3}$ Nms/rad/kg and $10.57\pm4.63\times10^{-3}$ Nms/rad/kg. In summary, our reported impedance during standing postures had similar values of DP stiffness during the stance phase of walking, but smaller values of DP damping.

In the frontal plane, the IE stiffness and IE damping during stance phase of walking ranges 1.5 Nms/rad/kg to 3.7 Nms/rad/kg and $18 \pm 26 \times 10^{-3}$ Nms/rad/kg to $50 \pm 29 \times 10^{-3}$ Nms/rad/kg [32], respectively. On the other hand, we reported the corresponding IE stiffness and IE damping to range 0.94 ± 0.27 Nm/rad/kg to 1.10 ± 0.40 Nm/rad/kg and $0.87 \pm 0.22 \times 10^{-3}$ Nms/rad/kg to $1.0 \pm 0.38 \times 10^{-3}$ Nms/rad/kg, respectively; Both below the corresponding walking counterparts. Further studies can verify if the differences of viscous damping between static postures and walking are related to joint movement [47] or muscle co-contraction [9], [28], [37]. However, preliminary work in the frontal plane has indicated that the IE stiffness and damping during standing are relatively invariant to muscle contraction [37].

E. Limitations

This study characterized the multi-directional ankle impedance during standing based on the assumption that the ankle is modeled as a 2nd order, linear system. While this assumption produces a model with a high %VAF, in reality, there may be additional nonlinear or higher-order dynamics that were not accounted for. Tehrani et al. recently suggested an ankle admittance with three poles and two zeros can better explain the intrinsic ankle dynamics when the ankle was not loaded, and no muscle activity was present [43]. Additionally, when muscle activity is substantial, the ankle impedance includes a component with a transport delay and a nonlinearity in the ankle velocity [44]. This work did not consider antiresonances in the impedance model or effects of the muscle contraction, which could be monitored with Electromyography measurements of the lower-leg muscles.

Using the experimental protocol defined in this paper, the COP of the foot was only varied along the long axis of the foot, from the heel toward the toes. We found it challenging to consistently vary the COP of the foot in the frontal plane while maintaining a stable stance. Consequently, this could explain why the IE stiffness did not changed noticeably across the four postures. Future work can improve upon the experimental design to increase the ankle torque and angle variation in the IE direction, and potentially investigate the varying IE ankle impedance. This could improve our understanding of how the ankle is modulated during turning or side-step maneuvers [48].

In addition, the subject population that participated in this experiment included young adult male subjects with no previous history of ankle injuries. The data collected from this

experiment describes the preliminary results of estimating the multi-directional ankle impedance during standing; however, it is limited in being able to represent the ankle impedance of all people. Future work will look to expand the subject population to include both male and female subjects at a broader range of ages and generate a more generalized understanding of standing ankle impedance.

F. Future Implications

The results of this study showed that the multi-directional ankle impedance during different static, standing postures had some comparable features to the ankle impedance during dynamic walking. Even though this study did not capture how the ankle impedance is modulated during a dynamic scenario, the results provide useful knowledge about the ankle impedance across the gait cycle, while using a simpler experimental procedure. This could be beneficial in working with people who have neuromuscular disorders or other physical impairment that would prevent them from being able to complete a gait test. Future work can aim to improve ways to understand the multi-directional ankle impedance during walking.

Furthermore, this work also provides implications to improve the design and control of ankle-foot prostheses. Ficanha et al. have developed a 2-DOF ankle-foot prosthesis, capable of controlling the ankle in the DP-IE space [49]. The results of this study can be used to improve how biomimetic prostheses are controlled, about multiple angle directions φ , for a given standing or walking posture.

V. CONCLUSION

This work characterizes the multi-direction ankle impedance across four standing postures that resembled instances within the stance phase of the gait cycle. As the COP of the foot moved forward, the stiffness increased mostly along the sagittal plane, while the damping increased substantially in both frontal and sagittal planes. Across all parameters, except the ankle stiffness during the FF posture, the values in the DP direction were substantially higher than in the IE direction. Additionally, the highest stiffness and damping values found in the anisotropic curves were tilted CCW from the DP axis. Last, the results of this study showed that the ankle impedance during standing postures responds differently than non-loaded and dynamic walking scenarios of corresponding ankle angles and torques. The stiffness range during standing postures was similar to that of walking tasks, while the damping was considerably smaller than that of walking and non-loaded tasks. This paper expands our understanding of the multi-directional ankle impedance to various standing postures, where the ankle is subjected to different combinations of angles, internal torques, and external forces from the ground. These new insights into how the ankle impedance adjusts for different scenarios can lead to further progress in clinical applications, rehabilitation, and assistive gait devices.

REFERENCES

- [1] R. E. Kearney and I. W. Hunter, "System identification of human joint dynamics.," *Critical reviews in biomedical engineering*, vol. 18, no. 1, pp. 55–87, 1990.
- [2] N. Hogan, "Impedance Control: An Approach to Manipulation: Part I—Theory," *J. Dyn. Sys., Meas., Control*, vol. 107, no. 1, pp. 1–7, Mar. 1985, doi: 10.1115/1.3140702.
- [3] M. R. Tucker *et al.*, "Control strategies for active lower extremity prosthetics and orthotics: a review," *Journal of NeuroEngineering and Rehabilitation*, vol. 12, no. 1, p. 1, Jan. 2015, doi: 10.1186/1743-0003-12-1.
- [4] A. Roy et al., "Robot-Aided Neurorehabilitation: A Novel Robot for Ankle Rehabilitation," IEEE Transactions on Robotics, vol. 25, no. 3, pp. 569–582, Jun. 2009, doi: 10.1109/TRO.2009.2019783.
- [5] C. L. Brockett and G. J. Chapman, "Biomechanics of the ankle," *Orthop Trauma*, vol. 30, no. 3, pp. 232–238, Jun. 2016, doi: 10.1016/j.mporth.2016.04.015.
- [6] I. W. Hunter and R. E. Kearney, "Dynamics of human ankle stiffness: Variation with mean ankle torque," *Journal of Biomechanics*, vol. 15, no. 10, pp. 747–752, Jan. 1982, doi: 10.1016/0021-9290(82)90089-6.
- [7] R. E. Kearney and I. W. Hunter, "Dynamics of human ankle stiffness: Variation with displacement amplitude," *Journal of Biomechanics*, vol. 15, no. 10, pp. 753–756, Jan. 1982, doi: 10.1016/0021-9290(82)90090-2.
- [8] P. L. Weiss, R. E. Kearney, and I. W. Hunter, "Position dependence of ankle joint dynamics—I. Passive mechanics," *Journal of Biomechanics*, vol. 19, no. 9, pp. 727–735, Jan. 1986, doi: 10.1016/0021-9290(86)90196-X.
- [9] P. L. Weiss, R. E. Kearney, and I. W. Hunter, "Position dependence of ankle joint dynamics—II. Active mechanics," *Journal of Biomechanics*, vol. 19, no. 9, pp. 737–751, Jan. 1986, doi: 10.1016/0021-9290(86)90197-1.
- [10] I. D. Loram and M. Lakie, "Direct measurement of human ankle stiffness during quiet standing: the intrinsic mechanical stiffness is insufficient for stability," *The Journal of Physiology*, vol. 545, no. 3, pp. 1041–1053, 2002.
- [11] M. Casadio, P. G. Morasso, and V. Sanguineti, "Direct measurement of ankle stiffness during quiet standing: implications for control modelling and clinical application," *Gait & posture*, vol. 21, no. 4, pp. 410–424, 2005.
- [12] P. Amiri and R. E. Kearney, "Ankle intrinsic stiffness changes with postural sway," *Journal of Biomechanics*, vol. 85, pp. 50– 58, Mar. 2019, doi: 10.1016/j.jbiomech.2019.01.009.
- [13] G. A. Ribeiro, E. Ficanha, L. Knop, and M. Rastgaar, "Impedance of the Human Ankle During Standing for Posture Control," 2018.
- [14] B. C. Glaister, J. A. Schoen, M. S. Orendurff, and G. K. Klute, "Mechanical Behavior of the Human Ankle in the Transverse Plane While Turning," *IEEE Transactions on Neural Systems and Rehabilitation Engineering*, vol. 15, no. 4, pp. 552–559, Dec. 2007, doi: 10.1109/TNSRE.2007.908944.
- [15] E. J. Rouse, L. J. Hargrove, E. J. Perreault, and T. A. Kuiken, "Estimation of Human Ankle Impedance During the Stance Phase of Walking," *IEEE Transactions on Neural Systems and Rehabilitation Engineering*, vol. 22, no. 4, pp. 870–878, Jul. 2014, doi: 10.1109/TNSRE.2014.2307256.
- [16] H. Lee and N. Hogan, "Time-Varying Ankle Mechanical Impedance During Human Locomotion," *IEEE Transactions* on Neural Systems and Rehabilitation Engineering, vol. 23, no. 5, pp. 755–764, Sep. 2015, doi: 10.1109/TNSRE.2014.2346927.
- [17] A. L. Shorter and E. J. Rouse, "Mechanical Impedance of the Ankle During the Terminal Stance Phase of Walking," *IEEE Transactions on Neural Systems and Rehabilitation*

- Engineering, vol. 26, no. 1, pp. 135–143, Jan. 2018, doi: 10.1109/TNSRE.2017.2758325.
- [18] E. M. Ficanha, G. A. Ribeiro, L. Knop, and M. Rastgaar, "Time-varying human ankle impedance in the sagittal and frontal planes during stance phase of walking," in *Robotics and Automation (ICRA)*, 2017 IEEE International Conference on, 2017, pp. 6658–6664.
- [19] E. Ficanha, G. Ribeiro, L. Knop, and M. Rastgaar, "Estimation of the Two Degrees-of-Freedom Time-Varying Impedance of the Human Ankle," *J. Med. Devices*, vol. 12, no. 1, Jan. 2018, doi: 10.1115/1.4039011.
- [20] A. L. Shorter and E. J. Rouse, "Ankle Mechanical Impedance During the Stance Phase of Running," *IEEE Transactions on Biomedical Engineering*, pp. 1–1, 2019, doi: 10.1109/TBME.2019.2940927.
- [21] P. L. Weiss, I. W. Hunter, and R. E. Kearney, "Human ankle joint stiffness over the full range of muscle activation levels," *Journal of Biomechanics*, vol. 21, no. 7, pp. 539–544, Jan. 1988, doi: 10.1016/0021-9290(88)90217-5.
- [22] I. D. Loram and M. Lakie, "Human balancing of an inverted pendulum: position control by small, ballistic-like, throw and catch movements," *The Journal of Physiology*, vol. 540, no. 3, pp. 1111–1124, 2002, doi: 10.1113/jphysiol.2001.013077.
- [23] I. D. Loram, S. M. Kelly, and M. Lakie, "Human balancing of an inverted pendulum: is sway size controlled by ankle impedance?," *The Journal of physiology*, vol. 532, no. 3, pp. 879–891, 2001.
- [24] D. A. Winter, A. E. Patla, F. Prince, M. Ishac, and K. Gielo-Perczak, "Stiffness Control of Balance in Quiet Standing," *Journal of Neurophysiology*, vol. 80, no. 3, pp. 1211–1221, Sep. 1998, doi: 10.1152/jn.1998.80.3.1211.
- [25] P. G. Morasso and V. Sanguineti, "Ankle muscle stiffness alone cannot stabilize balance during quiet standing," *Journal of Neurophysiology*, vol. 88, no. 4, pp. 2157–2162, 2002.
- [26] T. E. Sakanaka, J. Gill, M. D. Lakie, and R. F. Reynolds, "Intrinsic ankle stiffness during standing increases with ankle torque and passive stretch of the Achilles tendon," *PloS one*, vol. 13, no. 3, 2018.
- [27] H. Lee, H. I. Krebs, and N. Hogan, "Multivariable Dynamic Ankle Mechanical Impedance With Relaxed Muscles," *IEEE Transactions on Neural Systems and Rehabilitation Engineering*, vol. 22, no. 6, pp. 1104–1114, Nov. 2014, doi: 10.1109/TNSRE.2014.2313838.
- [28] H. Lee, H. I. Krebs, and N. Hogan, "Multivariable Dynamic Ankle Mechanical Impedance With Active Muscles," *IEEE Transactions on Neural Systems and Rehabilitation Engineering*, vol. 22, no. 5, pp. 971–981, Sep. 2014, doi: 10.1109/TNSRE.2014.2328235.
- [29] V. Nalam and H. Lee, "Development of a Two-Axis Robotic Platform for the Characterization of Two-Dimensional Ankle Mechanics," *IEEE/ASME Transactions on Mechatronics*, vol. 24, no. 2, pp. 459–470, Apr. 2019, doi: 10.1109/TMECH.2019.2892472.
- [30] H. Lee, E. J. Rouse, and H. I. Krebs, "Summary of Human Ankle Mechanical Impedance During Walking," *IEEE Journal of Translational Engineering in Health and Medicine*, vol. 4, pp. 1–7, 2016, doi: 10.1109/JTEHM.2016.2601613.
- [31] J. Perry and J. M. Burnfield, "Gait Analysis: Normal and Pathological Function," J Sports Sci Med, vol. 9, no. 2, p. 353, Jun. 2010.
- [32] E. Ficanha, G. A. Ribeiro, L. Knop, and M. R. Aagaah, "Estimation of the 2-DOF Time-Varying Impedance of the Human Ankle," 2017.
- [33] E. M. Ficanha, G. A. Ribeiro, L. Knop, and M. Rastgaar, "Time-varying impedance of the human ankle in the sagittal and frontal planes during straight walk and turning steps," in

- Rehabilitation Robotics (ICORR), 2017 International Conference on, 2017, pp. 1413–1418.
- [34] A. L. Shorter, S. Finucane, and E. J. Rouse, "Ankle Mechanical Impedance During Waling in Chronic Stroke: Preliminary Results," in 2019 IEEE 16th International Conference on Rehabilitation Robotics (ICORR), Jun. 2019, pp. 246–251, doi: 10.1109/ICORR.2019.8779436.
- [35] E. M. Ficanha, G. A. Ribeiro, and M. Rastgaar, "Design and evaluation of a 2-dof instrumented platform for estimation of the ankle mechanical impedance in the sagittal and frontal planes," *IEEE/ASME Transactions on Mechatronics*, vol. 21, no. 5, pp. 2531–2542, 2016.
- [36] M. P. Murray, A. B. Drought, and R. C. Kory, "Walking Patterns of Normal Men," *JBJS*, vol. 46, no. 2, pp. 335–360, Mar. 1964, Accessed: Apr. 10, 2020. [Online]. Available: https://journals.lww.com/jbjsjournal/Abstract/1964/46020/Walking_Patterns_of_Normal_Men.9.aspx.
- [37] G. A. Ribeiro, L. N. Knop, and M. Rastgaar, "Directional Mechanical Impedance of the Human Ankle During Standing Pose with Active Muscles (Accepted)," Paris, France, 2020.
- [38] R. H. Byrd, J. C. Gilbert, and J. Nocedal, "A trust region method based on interior point techniques for nonlinear programming," *Math. Program.*, vol. 89, no. 1, pp. 149–185, Nov. 2000, doi: 10.1007/PL00011391.
- [39] D. E. Farrar and R. R. Glauber, "Multicollinearity in Regression Analysis: The Problem Revisited," *The Review of Economics and Statistics*, vol. 49, no. 1, pp. 92–107, 1967, doi: 10.2307/1937887.
- [40] R. M. Warner, Applied Statistics: From Bivariate Through Multivariate Techniques, 2nd ed. SAGE Publications, Inc., 2013.
- [41] S. Plagenhoef, F. G. Evans, and T. Abdelnour, "Anatomical data for analyzing human motion," *Research quarterly for* exercise and sport, vol. 54, no. 2, pp. 169–178, 1983.
- [42] J. G. Reid and R. K. Jensen, "Human Body Segment Inertia Parameters: A Survey and Status Report," *Exercise and Sport Sciences Reviews*, vol. 18, no. 1, pp. 225–242, Jan. 1990.
- [43] E. Sobhani Tehrani, K. Jalaleddini, and R. E. Kearney, "Ankle Joint Intrinsic Dynamics is More Complex than a Mass-Spring-Damper Model," *IEEE Transactions on Neural Systems and Rehabilitation Engineering*, vol. 25, no. 9, pp. 1568–1580, Sep. 2017, doi: 10.1109/TNSRE.2017.2679722.
- [44] K. Jalaleddini, E. S. Tehrani, and R. Kearney, "A Subspace Approach to the Structural Decomposition and Identification of Ankle Joint Dynamic Stiffness," *IEEE Transactions on Biomedical Engineering*, vol. PP, no. 99, pp. 1–1, 2017, doi: 10.1109/TBME.2016.2604293.
- [45] T. B. Schön, A. Wills, and B. Ninness, "System identification of nonlinear state-space models," *Automatica*, vol. 47, no. 1, pp. 39–49, Jan. 2011, doi: 10.1016/j.automatica.2010.10.013.
- [46] R. E. Kearney, R. B. Stein, and L. Parameswaran, "Identification of intrinsic and reflex contributions to human ankle stiffness dynamics," *IEEE Transactions on Biomedical Engineering*, vol. 44, no. 6, pp. 493–504, Jun. 1997, doi: 10.1109/10.581944.
- [47] F. Popescu, J. M. Hidler, and W. Z. Rymer, "Elbow impedance during goal-directed movements," *Exp Brain Res*, vol. 152, no. 1, pp. 17–28, Sep. 2003, doi: 10.1007/s00221-003-1507-4.
- [48] E. M. Ficanha, M. Rastgaar, B. Moridian, and N. Mahmoudian, "Ankle angles during step turn and straight walk: Implications for the design of a steerable ankle-foot prosthetic robot," 2013.
- [49] E. M. Ficanha, G. A. Ribeiro, H. Dallali, and M. Rastgaar, "Design and Preliminary evaluation of a Two DOFs cable-Driven ankle-Foot Prosthesis with active Dorsiflexion– Plantarflexion and inversion–eversion," Frontiers in bioengineering and biotechnology, vol. 4, p. 36, 2016.